Journal of Power Sources 195 (2010) 1698–1705

Contents lists available at ScienceDirect

Journal of Power Sources

journal homepage: www.elsevier.com/locate/jpowsour

Effect of impurities and moisture on lithium bisoxalatoborate (LiBOB) electrolyte performance in lithium-ion cells☆

L. Yang[a], M.M. Furczon[b], A. Xiao[a], B.L. Lucht[a], Z. Zhang[b], D.P. Abraham[b,*]

[a] Department of Chemistry, University of Rhode Island, Kingston, RI 02881, United States
[b] Chemical Sciences and Engineering Division, Argonne National Laboratory, 9700 South Cass Ave., Argonne, IL 60439, United States

ARTICLE INFO

Article history:
Received 11 September 2009
Accepted 30 September 2009
Available online 9 October 2009

Keywords:
$LiB(C_2O_4)_2$
Reference electrode
NMR
FTIR

ABSTRACT

Electrolytes containing $LiB(C_2O_4)_2$ (LiBOB) salts are of increasing interest for lithium-ion cells for several reasons that include their ability to form a stable solid electrolyte interphase on graphite electrodes. However, cells containing these electrolytes often show inconsistent performance because of impurities in the LiBOB salt. In this work we compare cycling and impedance data from cells containing electrolytes with LiBOB that was obtained commercially and LiBOB purified by a rigorous recrystallization procedure. We relate the difference in performance to a lithium oxalate impurity that may be a residual from the salt manufacturing process. We also examine the reaction of LiBOB with water to determine the effect of salt storage in high-humidity environments. Although LiBOB electrolytes containing trace amounts (~100 ppm) of moisture appear relatively stable, higher moisture contents (~1 wt%) lead to observable salt decomposition resulting in the generation of $B(C_2O_4)(OH)$ and $LiB(C_2O_4)(OH)_2$ compounds that do not dissolve in typical carbonate solutions and impair lithium-ion cell performance.

1. Introduction

Among the many challenges limiting the application of lithium-ion batteries in plug-in hybrid and electric vehicles are calendar life, cycle life, and thermal stability. The performance degradation of lithium-ion cells upon aging can be, to a large extent, associated with the thermal instability of the electrolyte [1,2]. The process is usually linked to the thermal dissociation and hydrolytic instability of $LiPF_6$ [3]. For this reason, significant efforts have been directed toward the development of alternative salts for lithium-ion batteries [4]. One salt that has received significant attention is lithium bisoxalatoborate, $LiB(C_2O_4)_2$, typically abbreviated as LiBOB. The LiBOB salt has many advantages compared to $LiPF_6$ including superior thermal stability, increased safety, and a more stable solid electrolyte interphase (SEI) [5–7]. For instance, LiBOB can effectively stabilize the graphite anode surface even in pure propylene carbonate-based electrolytes [8]. However, the salt has several disadvantages that include lower ionic conductivity, especially at temperatures below 0 °C, lower rate capability that results from a higher cell impedance [9] and significant cell gassing [10].

One of the more troubling aspects of LiBOB is the inconsistency of cell performance resulting from batch to batch variations in the purity of salt obtained from the various synthesis and purification procedures [10–12]. LiBOB salt purity can have a significant and often detrimental effect on cell performance. In a recent article Xu et al. showed that impurities in the LiBOB salt degrade the cycle life of $LiNi_{0.85}Co_{0.1}Al_{0.05}O_2$-bearing large-format (8Ah) cells, especially at elevated temperatures [10]. Their data from ^1H, ^{11}B and ^{13}C NMR spectra indicated the presence of oxalate and carboxylate impurities, which apparently decomposed and generated sufficient gas pressure to vent the cell. The authors also showed that cells containing purified (recrystallized) LiBOB display significantly improved cycling behavior and thermal stability characteristics. Depending on the mode of salt synthesis trace amounts of diethyl oxalate, acetonitrile, ethyl acetate, and hydrogen bis(oxalato)borate could also be present in LiBOB. For instance, Wang et al. identified HBO_2, HC_2O_4Li, and water in X-ray diffraction patterns of LiBOB prepared by a solid state reaction technique that employed heating mixtures of oxalic acid dihydrate, lithium hydroxide, and boric acid [13]. Residual amounts of water, resulting from its use as a solvent during LiBOB preparation, could also impair performance by reacting with the various cell components [14].

In this article we show electrochemical data from cells containing *commercial* LiBOB (*c*-LiBOB) and *purified* LiBOB (*p*-LiBOB).

☆ The submitted manuscript has been created by UChicago Argonne, LLC, Operator of Argonne National Laboratory ("Argonne"). Argonne, a U.S. Department of Energy Office of Science laboratory, is operated under Contract No. DE-AC02-06CH11357. The U.S. Government retains for itself, and others acting on its behalf, a paid-up nonexclusive, irrevocable worldwide license in said article to reproduce, prepare derivative works, distribute copies to the public, and perform publicly and display publicly, by or on behalf of the Government.

* Corresponding author. Tel.: +1 630 252 4332; fax: +1 630 972 4406.
E-mail address: abraham@anl.gov (D.P. Abraham).

0378-7753/$ – see front matter © 2009 Elsevier B.V. All rights reserved.
doi:10.1016/j.jpowsour.2009.09.056

Cycling behavior from coin cells and impedance behavior from cells containing a reference electrode are presented to show the differences in performance resulting from LiBOB quality. Nuclear magnetic resonance spectroscopy (NMR), Fourier transform infrared spectroscopy (FTIR) and thermogravimetric analysis (TGA) were used to identify the LiBOB impurities. The effect of moisture on LiBOB behavior and performance was also examined to determine the consequences of improper storage (in high-humidity environments, for example) after salt preparation. FTIR data and variable temperature NMR data were obtained on LiBOB samples soaked in water for various time periods. Based on our data we suggest measures to ensure salt quality, which in turn would enhance the performance of lithium-ion cells containing LiBOB electrolytes.

2. Experimental

For our experiments we either used LiBOB secured from a commercial source or LiBOB that was purified in the following manner. 30 g of *c*-LiBOB was placed in a 500 ml beaker, and then 150 ml anhydrous acetonitrile was added to dissolve the powder (the acetonitrile was previously dried by refluxing in CaH_2 for 24 h). The mixture was heated to 40 °C and gently stirred to obtain a supersaturated solution of LiBOB in acetonitrile. The solution was then filtered to remove impurities and excess salt, which were retained on the filter paper. The resulting clear LiBOB + acetonitrile solution was then mixed with 150 ml cold toluene. Crystalline precipitates of LiBOB were immediately observed in solution because the salt has negligible solubility in toluene. After 0.5 h, the solid precipitates were filtered out and placed in vacuum to remove residual acetonitrile and toluene; the yield of this purification process was about 80%. The resulting LiBOB powder was finally dried in a vacuum oven at 130 °C for 15 h.

An important difference between the *c*-LiBOB and *p*-LiBOB was in their solubilities. The *c*-LiBOB did not dissolve in a ethylene carbonate (EC): ethyl methyl carbonate (EMC) (3:7, by wt) solvent mixture even after a week; however, the salt dissolved in a EC: diethyl carbonate (DEC) (1:1 by wt) mixture in about 24 h. In contrast, the *p*-LiBOB dissolved in the 3EC:7EMC solvent within minutes. It is apparent, therefore, that impurities inhibit the dissociation, and hence dissolution of *c*-LiBOB in the 3EC:7EMC solvent.

The commercial and purified LiBOB samples were analyzed by FTIR-ATR, TGA and NMR to identify the impurities. FTIR measurements of solid samples were obtained on a Thermo Nicolet Magna 550 spectrometer stored in a glove bag that was purged with highly pure Ar. The spectra were acquired in the Attenuated Total Reflection (ATR) mode with 4 cm^{-1} resolution and 128 total scans. The TGA data were collected on a TA Instruments SDT 2900 by ramping the temperature from room temperature to 600 °C at a rate of 10 °C min^{-1}. The ^{1}H, ^{13}C and ^{11}B NMR data were collected on liquid samples with a JEOL 400 MHz NMR spectrometer; the spectra were acquired either in 3EC:7EMC solvent or in D_2O. The ^{11}B NMR data were referenced to $BF_3{\cdot}O(C_2H_5)$ at 0 ppm.

The positive electrode used for the electrochemical studies was prepared by coating a mixture of 84 wt% $LiNi_{0.8}Co_{0.15}Al_{0.05}O_2$ (NCA), 4 wt% SFG-6 graphite, 4 wt% acetylene black and 8 wt% PVdF binder on a 30-μm thick Al foil. The coating thickness was 35 μm and the oxide loading density was 8 mg cm^{-2}. The negative electrode was prepared by coating a mixture of 91 wt% Mag-10 graphite and 9 wt% PVdF binder on a 18-μm thick Cu foil. The coating thickness was 35 μm, and the graphite loading density was 4.9 mg cm^{-2}. The electrolytes used to study the electrochemical performance of cells contained either 0.7 M *c*-LiBOB or 0.7 M *p*-LiBOB in 1EC:1DEC (by wt) solvent. A 25-μm thick tri-layer separator (Celgard 2325) provided electronic isolation between the electrodes.

Electrochemical data were obtained both from 2032-type coin cells (1.6 cm^2 area electrodes) and from larger cells (32 cm^2 area electrodes) that incorporated a Li–Sn reference electrode. Details of the Li–Sn reference electrode preparation and cell assembly are discussed elsewhere [15,16]. The coin cells were typically cycled in a controlled temperature oven held at 30 °C. The reference electrode cells were assembled and tested in an inert-atmosphere glove box (O_2, H_2O < 1 ppm) to minimize the impact of moisture and oxygen. In general, the cycling ranges for NCA//Li, graphite//Li and NCA//graphite cells were 3–4.3 V vs. Li, 1.5–0 vs. Li, and 3–4.1 V, respectively. All impedance data were collected on the NCA//graphite reference electrode cells. Electrochemical Impedance Spectroscopy (EIS) measurements were conducted with an EG&G 273A potentiostat and a Solartron SI1260 frequency response analyzer controlled by ZPLOT measurement software. Data for the full cell, positive electrode vs. Li–Sn, and negative electrode vs. Li–Sn were collected in the potentiostatic mode, in the 25 kHz to 10 mHz frequency range, with a 10-mV perturbation about the open-circuit voltage. The measurements were typically conducted at a full cell voltage of 3.72 V.

3. Results and discussion

3.1. Electrochemical cycling and impedance measurements

Fig. 1 shows differential capacity plots of the first lithiation–delithiation cycle from graphite//Li cells with electrolytes containing the commercial and purified LiBOB. During the first lithiation, both cells show peaks at voltages greater than 1.5 V; the peak for the *c*-LiBOB cell is shorter and at a lower voltage (1.68 V) than the *p*-LiBOB cell (1.75 V). These peaks were not observed during subsequent graphite lithiation–delithiation cycles, and are apparently associated with the reduction of a LiBOB salt component that is reduced during the first lithiation cycle. The shorter peak for the *c*-LiBOB cell suggests that impurities inhibit reduction of this LiBOB salt component. Electrolyte reduction for both cells is relatively minor between 1.5 and 1 V but increases at lower voltages with both cells showing peaks in the ~0.6 to 0.8 V range. The presence of these lower voltage peaks indicates that the high-voltage (>1.5 V) electrolyte reduction does not sufficiently passivate the graphite surface. Again, these peaks are observed

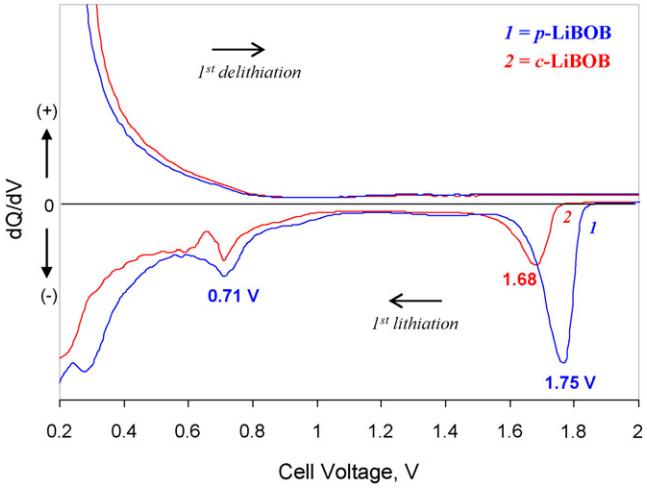

Fig. 1. Differential capacity plots from graphite//Li cells with electrolytes containing the commercial LiBOB (*c*-LiBOB) and purified LiBOB (*p*-LiBOB). The X-axis voltage range is limited to highlight electrolyte reduction processes. The main graphite lithiation–delithiation peaks, at voltages less than ~0.2 V, are beyond the scale of this plot.

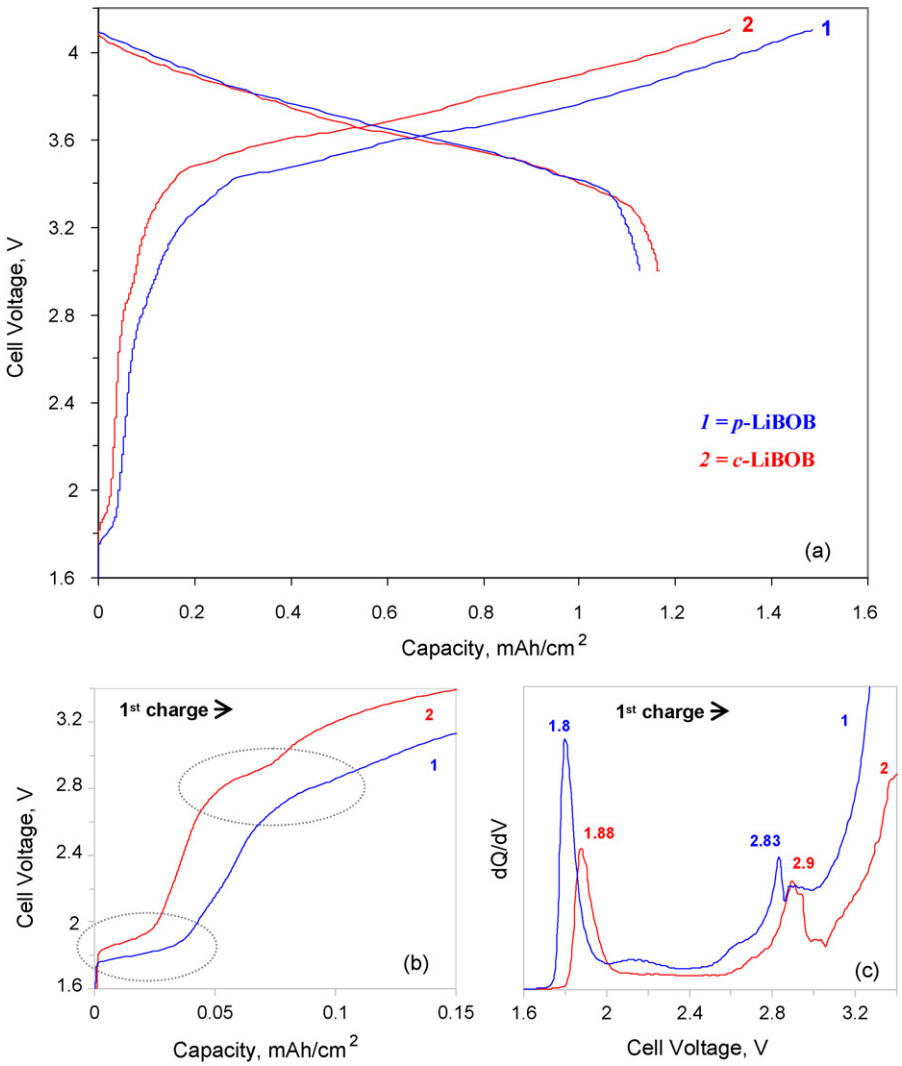

Fig. 2. (a) First cycle data from NCA//graphite cells with electrolytes containing the *c*-LiBOB and *p*-LiBOB (b) is the expanded view of (a) showing plateaus in capacity–voltage curve, and (c) is the differential capacity plot of data shown in (b).

only during the first graphite-lithiation, and not in subsequent delithiation–lithiation cycles.

Fig. 2a contains capacity–voltage plots from NCA//graphite cells with electrolytes containing the *c*-LiBOB and *p*-LiBOB. The *p*-LiBOB cell polarizes less and displays a higher charge capacity than the *c*-LiBOB, but the discharge capacities are similar. In the early part of the charge curve (~1.8 to 1.9 V), the *c*-LiBOB cell displays a shorter voltage plateau than the *p*-LiBOB cell. These plateaus are clearly seen in Fig. 2b, and appear as peaks in Fig. 2c, which contain the corresponding differential capacity plots. Both cells show peaks in Fig. 2c in the 2.8–3 V range. By accounting for the charge moved through the cells we could correlate the 1.8–1.9 V range peaks to the higher voltage (>1.5 V) peak in the graphite/Li cell data (Fig. 1). Furthermore, the ~2.8 to 3 V peaks in the NCA//graphite cells are akin to the ~0.6 to 0.8 V peaks in the graphite/Li cell data. That is, peaks at voltages less than ~3.2 V in Fig. 2 are related to electrolyte reduction processes at the graphite negative electrode. In general, the differences in cell behavior observed in Fig. 2 may be attributed to impurities in the *c*-LiBOB salt.

Fig. 3 shows impedance data obtained on the full cell, and on individual positive and negative electrodes from cells containing electrolytes with the commercial or purified LiBOB salts; the area specific impedance (in ohm-cm^2) data are based on geometric area (32 cm^2) of the electrodes. Some of the data display a high-frequency tail (>1 kHz) that is a spurious capacitive effect arising from interaction of the measuring instrumentation with the low-impedance cell. The mid-frequency arc, at frequencies between ~1 kHz and ~1 Hz, is related to electrode-electrolyte interfacial processes, and the low-frequency sloping line (Warburg tail), at frequencies less than ~1 Hz, is mainly related to diffusion processes in the electrolyte and through the active material particles. From the data it is evident that the impedance of the *c*-LiBOB cell is larger than that of the *p*-LiBOB cell. The main effect is on the mid-frequency arc on the negative electrode, which indicates that the impurity affects the graphite electrode-electrolyte interface, i.e. characteristics of the graphite SEI. A small effect is also observed at the positive electrode interface, which suggests that surface films on this electrode are also affected by the impurity.

3.2. NMR and IR spectroscopic analysis of LiBOB salts

The structure of soluble organic components in liquid samples can be characterized by NMR spectroscopy. Fig. 4 contains ^{1}H, ^{13}C, and ^{11}B NMR spectra obtained from *p*-LiBOB salt dissolved in 3EC:7EMC solvent. The ^{1}H spectrum showed contributions only from the EC and EMC components, which is as expected because

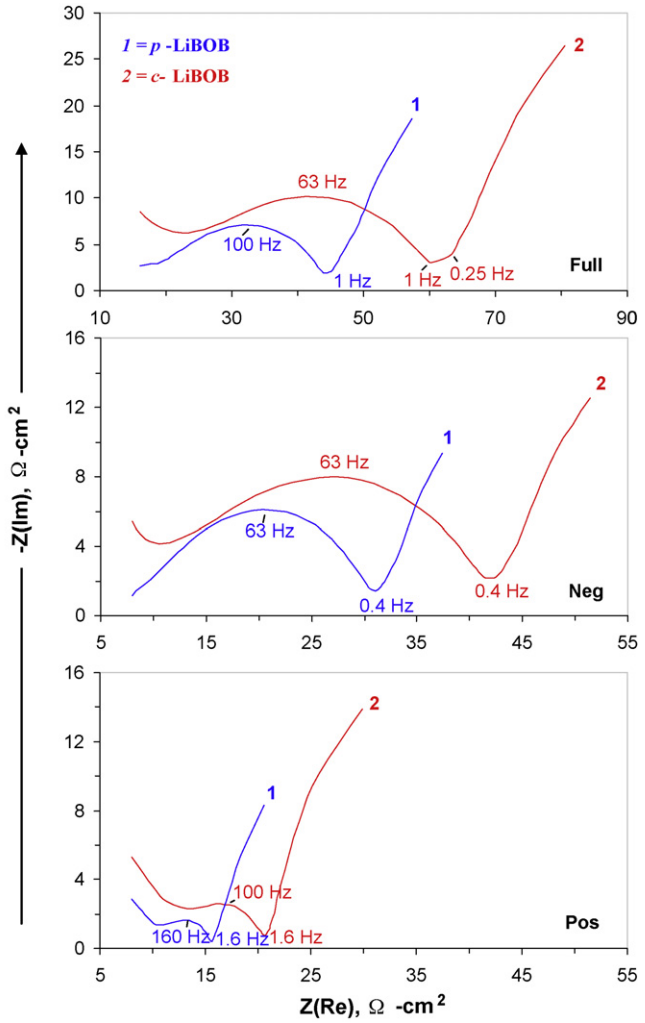

Fig. 3. EIS data (30 °C, 25 kHz to 0.01 Hz) data from NCA//graphite cells with electrolytes containing the *c*-LiBOB and *p*-LiBOB. The full cell, positive electrode and negative electrode data were obtained at a full cell potential of 3.72 V.

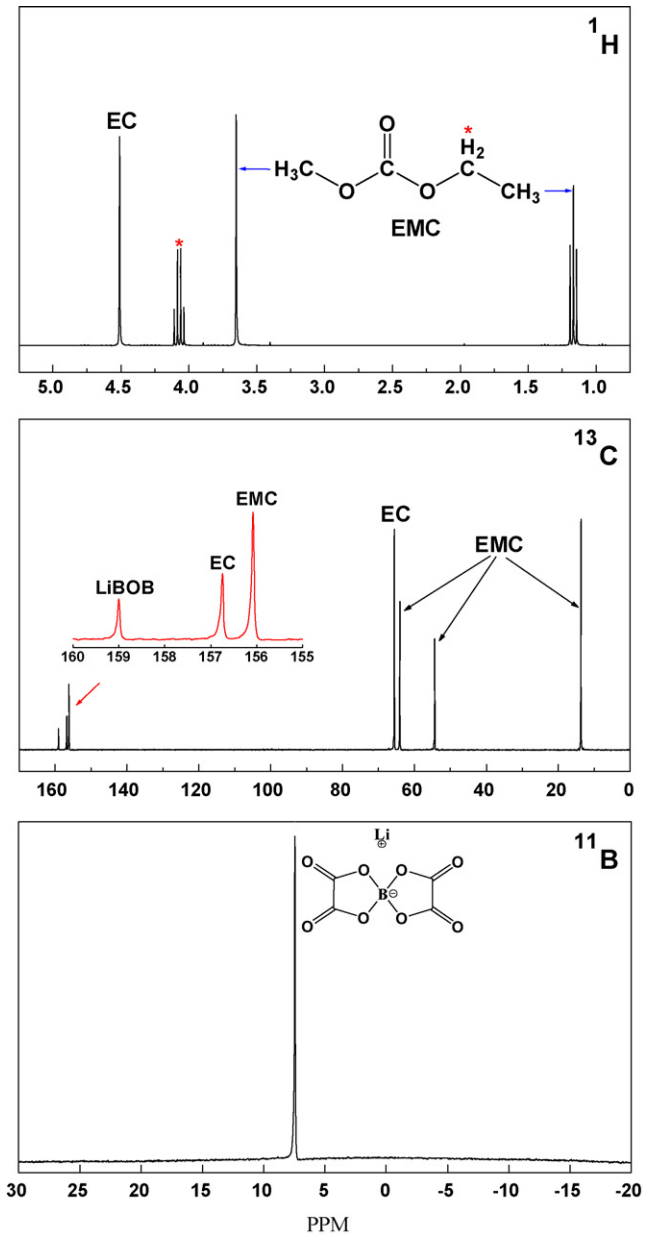

Fig. 4. ^{1}H, ^{13}C, and ^{11}B NMR spectra obtained from *p*-LiBOB salt dissolved in 3EC:7EMC solvent. Similar data were obtained with the *c*-LiBOB salts.

there are no protons in the pure BOB anion. The ^{13}C spectrum displayed features associated with EC, EMC, and the BOB anion, and the ^{11}B spectrum contained contributions from the BOB anion [12]. The spectra from the *c*-LiBOB samples were very similar to those shown in Fig. 4. Features corresponding to compounds such as ethyl acetate in the ^{1}H and ^{13}C spectra, and that from a B-bearing impurity in the ^{11}B spectrum reported by Xu et al. [10], were not observed.

Fig. 5 shows FTIR spectra of the *p*-LiBOB and *c*-LiBOB salts. The *p*-LiBOB spectrum contains several strong absorptions in the C=O stretching region (1740–1820 cm^{-1}) and in the C–O and B–O stretching regions (980–1370 cm^{-1}), which are consistent with previously published LiBOB spectra [17,18]. The *c*-LiBOB spectrum contains additional absorptions at 1658 and 778 cm^{-1}, which are consistent with the presence of lithium oxalate in the sample.

Fig. 6 shows TGA data from the *p*-LiBOB and *c*-LiBOB salts. The weight change data (Fig. 6a) shows that the *c*-LiBOB has a higher onset temperature for decomposition and lower weight loss in the 300–400 °C range. The weight change derivative (Fig. 6b) shows a single low temperature peak for *p*-LiBOB, but two peaks for *c*-LiBOB. The lower peak (~350 °C) in the *c*-LiBOB data corresponds to the pure LiBOB salt, whereas the higher peak (~370 °C) is consistent with the presence of mixed aggregates or co-crystals of LiBOB with an impurity compound. Mixed aggregates of lithium salts have been described previously and are known to alter physical properties of the pure compounds [19]. The peaks in the 450–525 °C range, seen in both the *p*-LiBOB and *c*-LiBOB data, are from the thermal decomposition of lithium oxalate; these peaks are slightly larger in the *c*-LiBOB data.

To determine the identity of the impurity compound we isolated the portion of *c*-LiBOB that was insoluble in 3EC:7EMC solvent. FTIR-ATR spectrum of this insoluble residue contained significant absorptions at 1658, 1328, and 775 cm^{-1} (Fig. 7), which are characteristic of $Li_2C_2O_4$. The minor absorptions at 1740–1820 cm^{-1} and 980–1370 cm^{-1} are consistent with low concentrations of EC and/or LiBOB. The ^{13}C NMR spectrum, obtained after dissolving the residue in D_2O, contained a single resonance at 168 ppm (Fig. 8), characteristic of $Li_2C_2O_4$. The absence of absorptions at 156 and 56 ppm for EC and 158 ppm for LiBOB (see Fig. 8) indicate that the residue is primarily lithium oxalate.

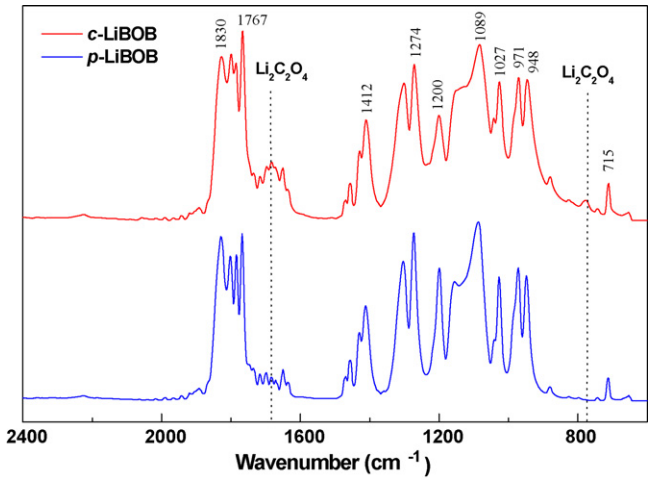

Fig. 5. FTIR spectra from *p*-LiBOB and *c*-LiBOB salts.

3.3. Effect of water on LiBOB salts and electrolytes

Water is known to impair the performance of lithium-ion cells, especially those containing $LiPF_6$-bearing electrolytes. In contrast, LiBOB-bearing electrolytes containing trace amounts of water (~100 ppm) are known to be relatively stable [20]. Zavalij et al. have shown that unsolvated LiBOB is highly hygroscopic, forming a hydrate that loses water above 110 °C [21]. Herein, we discuss the property and performance of LiBOB-electrolytes containing relatively high moisture contents (~1 wt%), which could result from salt or electrolyte storage in high-humidity environments.

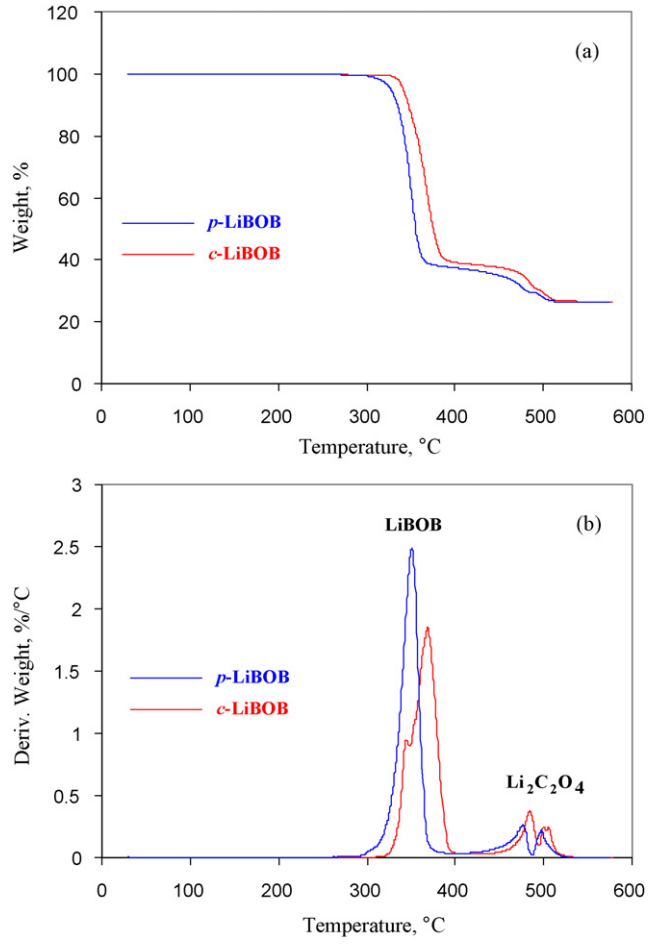

Fig. 6. TGA data showing (a) weight change and (b) derivate of weight change data obtained on *p*-LiBOB and *c*-LiBOB salts.

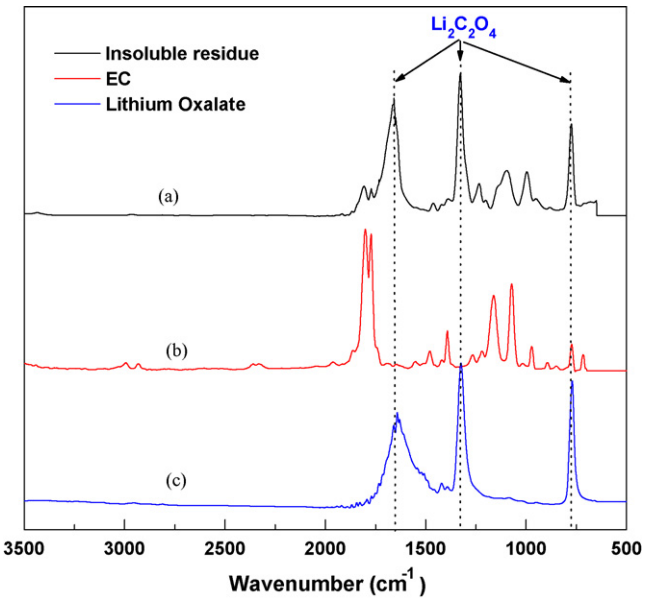

Fig. 7. FTIR spectra from (a) *c*-LiBOB residue after attempted dissolution in 3EC:7EMC solvent, (b) ethylene carbonate, and (c) lithium oxalate.

The *p*-LiBOB salt was exposed to 100% humidity at RT for 12 h to generate *wet* LiBOB (*w*-LiBOB). The FTIR spectrum of *w*-LiBOB shows new absorptions between 3600 and 3000 cm^{-1} consistent with the generation of O–H bonds (Fig. 9). In addition, when compared to *p*-LiBOB data, the *w*-LiBOB spectrum shows a shift in many of the absorptions between 1500 and 800 cm^{-1} that suggest changes in material structure. Attempted dissolution of *w*-LiBOB in 3EC:7EMC resulted in only partial solubility of the salt. An FTIR spectrum of the insoluble residue showed absorptions in the C=O stretching region (1740–1820 cm^{-1}) and in the C–O and B–O stretching regions (980–1370 cm^{-1}) consistent with the presence

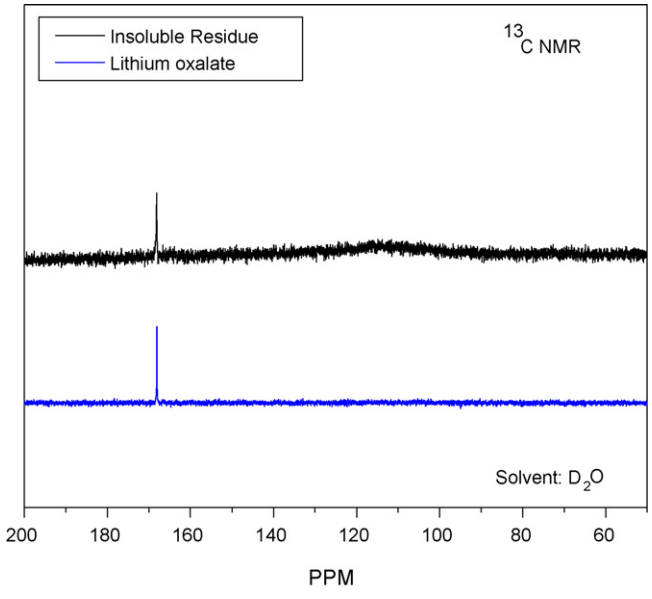

Fig. 8. ^{13}C NMR spectra from (a) *c*-LiBOB residue after attempted dissolution in 3EC:7EMC solvent, (b) lithium oxalate.

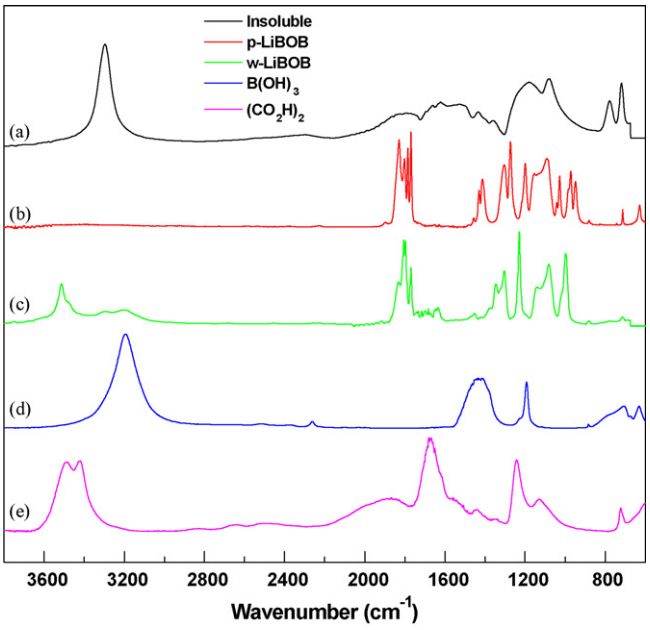

Fig. 9. FTIR spectra from (top to bottom): (a) *insoluble* component after attempted dissolution of *w*-LiBOB in 3EC:7EMC solvent, (b) *p*-LiBOB, (c) *w*-LiBOB, (d) $B(OH)_3$, and (e) oxalic acid.

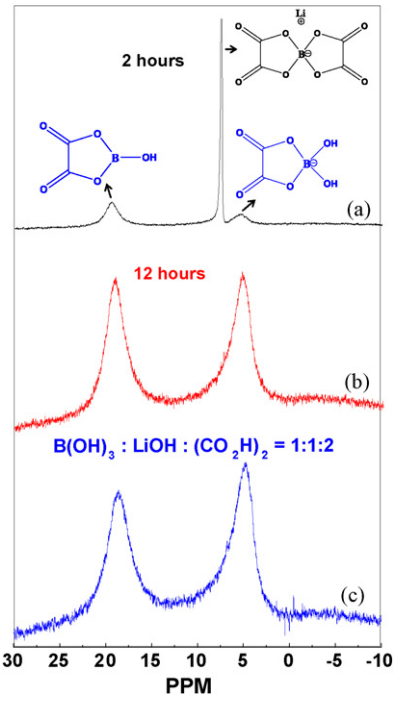

Fig. 11. ^{11}B NMR spectra of *p*-LiBOB in water after (a) 2 h and (b) 12 h. (c) ^{11}B spectrum of $B(OH)_3$:LiOH:oxalic acid (1:1:2) mixture in water.

of boron coordinated to oxalate ligands (Fig. 9); the strong absorption at 3300 cm^{-1} is indicative of OH presence. Fig. 9 shows that the wavelength and shape of these peaks do not match either $B(OH)_3$ or $(CO_2H)_2$, i.e., the spectra indicate the presence of other boron and hydroxide bearing compounds.

The ^{11}B NMR spectrum of *w*-LiBOB in 3EC:7EMC solvent (Fig. 10) shows broad peaks at ~4.5 and ~20 ppm in addition to the main LiBOB peak at ~7 ppm. The 4.5 ppm peak is similar to the impurity peak reported by Xu et al. [10] To determine the identity of these additional peaks we investigated the reaction of the *p*-LiBOB salt with water. Upon soaking, the LiBOB salt quickly reacts with water to generate two new broad ^{11}B NMR resonances at ~5 and ~20 ppm (Fig. 11a), which are very similar to the resonances observed upon exposure of LiBOB to high-humidity (Fig. 10); the small differences in chemical shift can be attributed to differences in solvent (3EC:7EMC in Fig. 10 and water in Fig. 11). The spectrum after a 12 h soak shows peaks at 5 and 20 ppm only; the 7 ppm resonance characteristic of LiBOB is absent, which indicates a complete conversion of the salt into two other species (Fig. 11b). We suggest that the two new resonances are from $B(C_2O_4)(OH)$ at 20 ppm and $LiB(C_2O_4)(OH)_2$ at 5 ppm. To allow independent confirmation of these peak assignments, we prepared mixtures of $B(OH)_3$ with varying concentrations of added LiOH and oxalic acid $(CO_2H)_2$ in water, which result in the generation of $B(C_2O_4)(OH)$ and $LiB(C_2O_4)(OH)_2$. Fig. 11c shows that the ^{11}B NMR spectrum of a mixture containing $B(OH)_3$:LiOH:oxalic acid (1:1:2) is very similar to Fig. 11b, which is the spectrum of *p*-LiBOB in water after a 12 h soak.

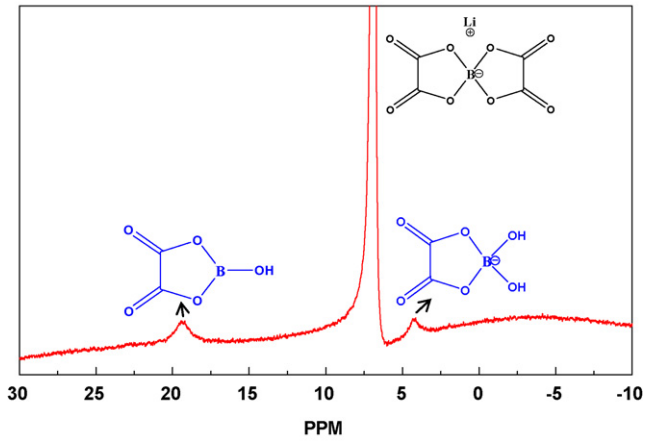

Fig. 10. ^{11}B NMR spectrum of *w*-LiBOB in 3EC:7EMC solvent. Peaks at ~4.5 and ~20 ppm are seen in addition to the LiBOB peak at ~7 ppm.

The broadness of the ^{11}B signals suggest a continuous exchange of the two species, which was confirmed by variable temperature NMR spectroscopy. Fig. 12 shows that the relative height and width of the $LiB(C_2O_4)(OH)_2$ and $B(C_2O_4)(OH)$ peaks vary reversibly with temperature. The peak intensities are comparable at 25 °C, but the 5 ppm peak is more intense at 5 °C and almost non-existent at 60 °C. Based on these data we propose Scheme 1 for the LiBOB–water reaction.

The resonances from $LiB(C_2O_4)(OH)_2$ and $B(C_2O_4)(OH)$ are likely present in the ^{11}B NMR spectrum of LiBOB-carbonate solutions containing small amounts (~100 ppm) of water, but are undetectable due to the low concentrations and peak broadening effects. However, larger amounts (~1 wt%) of water added to LiBOB-carbonate solutions produce observable concentrations of $B(C_2O_4)(OH)$ and $LiB(C_2O_4)(OH)_2$ according to reactions shown in the above schematic. Fig. 13 shows capacity vs. cycle number plots from NCA//graphite cells with electrolytes containing the *p*-LiBOB and *w*-LiBOB salts in 1EC:1DEC solvent. The *w*-LiBOB salt did not fully dissolve in the solvent and generated a cloudy solution. The data indicate that the *w*-LiBOB cell takes longer to achieve full capacity probably because of factors associated with electrode wetting. In addition, the *w*-LiBOB cell displays a lower capacity that may result from additional SEI formation reactions associated with the $B(C_2O_4)(OH)$ and $LiB(C_2O_4)(OH)_2$ compounds in the electrolyte.

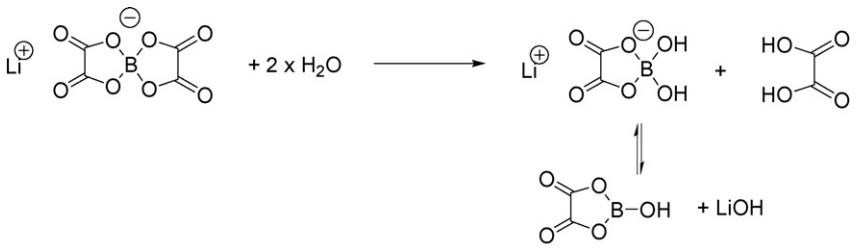

Scheme 1.

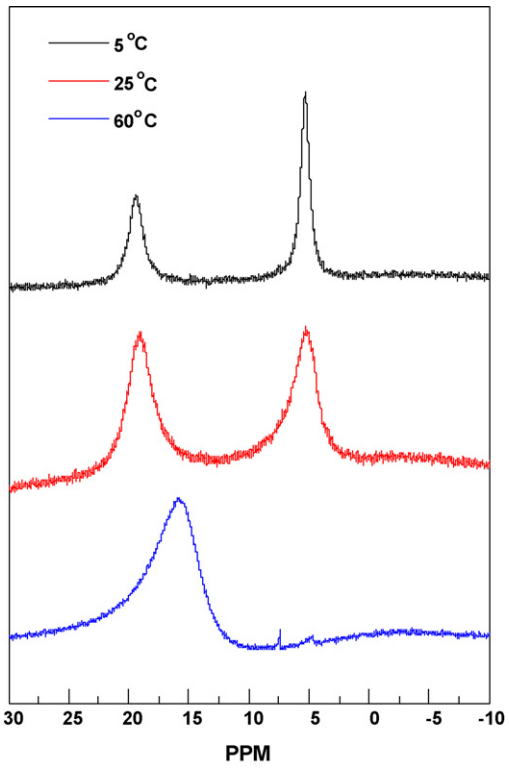

Fig. 12. ^{11}B NMR spectra of *p*-LiBOB soaked in water for 12 h obtained at 5 °C, 25 °C, and 60 °C. The peak at 20 ppm is from $B(C_2O_4)(OH)$ and the peak at 5 pm is from $LiB(C_2O_4)(OH)_2$. The reversible exchange of the two species results in peak broadening.

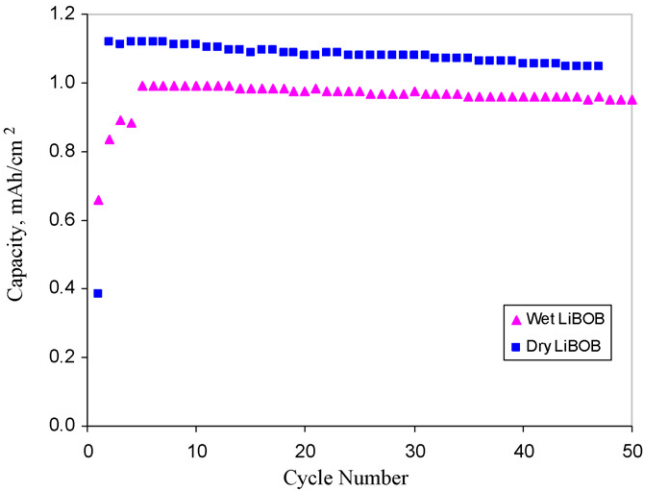

Fig. 13. Capacity vs. cycle number data for NCA//graphite cells with electrolytes containing the dry and wet LiBOB in 1EC:1DEC solvent. The cycling current densities were 0.047 mA cm^{-2} (1st cycle), 0.094 mA cm^{-2} (2nd and 3rd cycles), and 0.189 mA cm^{-2} for the remaining cycles.

4. Conclusions

The commercial LiBOB studied in our experiments contained a small amount of lithium oxalate ($Li_2C_2O_4$) impurity. This lithium oxalate is likely a residual from the manufacturing process as opposed to being generated by exposure to air after salt preparation. The separation of the LiBOB and $Li_2C_2O_4$ is most likely complicated by the formation of co-crystals or mixed aggregates. The presence of this impurity inhibits the dissolution of LiBOB into a 3EC:7EMC solvent mixture and increases the impedance of lithium-ion cells. Storage of LiBOB salts in high-humidity environments can lead to salt decomposition resulting in the generation of $B(C_2O_4)(OH)$ and $LiB(C_2O_4)(OH)_2$ compounds, which do not dissolve in typical carbonate solutions. In order to maintain proper quality control of LiBOB-based electrolytes, we suggest two primary measures. First, one should investigate the solubility of the LiBOB salt in carbonate solvents, such as EC:EMC. There may be impurities present in the salt if the LiBOB does not readily dissolve in the solvents. FTIR spectroscopy is a relatively straightforward technique to determine LiBOB purity. The presence of absorptions at ~1658 and ~775 cm^{-1} would suggest the presence of lithium oxalate impurities associated with the salt manufacturing process. Alternatively, absorptions at 3300 cm^{-1} would suggest the presence of boric acids that could arise from improper storage of the salts or electrolytes.

Acknowledgments

This work was supported by the U.S. Department of Energy (DOE), Office of Vehicle Technologies. We are grateful for the support of Dave Howell at DOE, and Gary Henriksen, Dennis Dees and Andrew Jansen at Argonne. This manuscript has been created by UChicago Argonne, LLC, Operator of Argonne National Laboratory ("Argonne"). Argonne, a U.S. Department of Energy Office of Science laboratory, is operated under Contract No. DE-AC02-06CH11357.

References

[1] S.E. Sloop, J.B. Kerr, K. Kinoshita, J. Power Sources 119–121 (2003) 330–337.
[2] D. Aurbach, J. Power Sources 119–121 (2003) 497–503.
[3] L.C. Christopher, L. Wentao, L.L. Brett, J. Electrochem. Soc. 152 (2005) A2327–A2334.
[4] K. Xu, Chem. Rev. 104 (2004) 4303–4418.
[5] K. Xu, S.S. Zhang, T.R. Jow, W. Xu, C.A. Angell, Electrochem. Solid State Lett. 5 (2002) A26–A29.
[6] J.C. Panitz, U. Wietelmann, M. Wachtler, S. Strobele, M. Wohlfahrt-Mehrens, J. Power Sources 153 (2006) 396–401.
[7] J. Jiang, J.R. Dahn, Electrochem. Solid State Lett. 6 (2003) A180–A182.
[8] K. Xu, S.S. Zhang, B.A. Poese, T.R. Jow, Electrochem. Solid State Lett. 5 (2002) A259–A262.
[9] D.P. Abraham, M.M. Furczon, S.-H. Kang, D.W. Dees, A.N. Jansen, J. Power Sources 180 (2008) 612–620.
[10] K. Xu, B. Deveney, K. Nechev, Y. Lam, T.R. Jow, J. Electrochem. Soc. 155 (2008) 959–964.
[11] M. Wachtler, M. Wohlfahrt-Mehrens, S. Strobele, J.C. Panitz, U. Wietelmann, J. Appl. Electrochem. 36 (2006) 1199–1206.
[12] X. Wu, C.A. Angell, Electrochem. Solid-State Lett. 4 (2001) E1–E4.

[13] S. Wang, W. Qiu, T. Li, B. Yu, H. Zhao, Int. J. Electrochem. Sci. 1 (2006) 250–257.
[14] H.G. Schweiger, M. Multerer, U. Wietelmann, J.-C. Panitz, T. Burgemeister, H.J. Gores, J. Electrochem. Soc. 152 (2005) A622–A627.
[15] D.P. Abraham, S.D. Poppen, A.N. Jansen, J. Liu, D.W. Dees, Electrochim. Acta 49 (2004) 4763–4775.
[16] D.P. Abraham, E.M. Reynolds, P.L. Schultz, A.N. Jansen, D.W. Dees, J. Electrochem. Soc. 153 (2006) A1610–A1616.
[17] G.V. Zhuang, K. Xu, T.R. Jow, P.N. Ross, Electrochem. Solid State Lett. 7 (2004) A224–A227.
[18] B.T. Yu, W.H. Qiu, F.S. Li, G.X. Xu, Electrochem. Solid State Lett. 9 (2006) A1–A4.
[19] K.J. Singh, D.B. Collum, J. Am. Chem. Soc. 128 (2006) 13753–13760.
[20] A. Xiao, L. Yang, B.L. Lucht, Electrochem. Solid State Lett. 10 (2007) A241–A244.
[21] P.Y. Zavalij, S. Yang, M.S. Whittingham, Acta Crystallogr. Section B-Struct. Sci. 60 (2004) 716–724.